

Optics Letters

Three-dimensional direct laser written achromatic axicons and multi-component microlenses

MICHAEL SCHMID,^{1,*} SIMON THIELE,² ALOIS HERKOMMER,² AND HARALD GIESSEN¹

¹4th Physics Institute and Research Center SCoPE, University of Stuttgart, Pfaffenwaldring 57, 70569 Stuttgart, Germany

²Institute of Applied Optics (ITO) and Research Center SCoPE, University of Stuttgart, Pfaffenwaldring 9, 70569 Stuttgart, Germany

*Corresponding author: m.schmid@pi4.uni-stuttgart.de

Received 24 September 2018; revised 30 October 2018; accepted 31 October 2018; posted 5 November 2018 (Doc. ID 345260); published 29 November 2018

Femtosecond 3D printing is an important technology for manufacturing nano- and microscopic optical devices and elements. However, most structures in the past have been created using only one photoresist at a time, thus limiting potential applications. In this Letter, we successfully demonstrate the combination of two different photoresists, namely, IP-S and IP-Dip, to realize multi-component three-dimensional direct laser written optics. We use the combination of IP-S and IP-Dip to correct chromatic aberrations and to realize an achromatic axicon. In a second step, we demonstrate, to the best of our knowledge, the first three-dimensional direct laser written Fraunhofer doublet. We characterize their optical properties and measure the substantial reduction in chromatic aberrations. We outline the possibilities and benefits of creating three-dimensional direct laser written multi-component structures for micro-optics. © 2018 Optical Society of America

<https://doi.org/10.1364/OL.43.005837>

3D direct laser writing is an important state-of-the-art technology for manufacturing nano- and micro-optical devices and elements [1–18]. Over the last years, the large potential of 3D direct laser written optics and possible applications, e.g., in endoscopy or sensing, have been investigated [1–4].

However, most structures have been created using one photoresist at a time, limiting optical performance and possible applications. For optical performance, it is crucial to minimize aberrations, such as defocus, spherical aberration, coma, astigmatism, field curvature, or image distortion. 3D direct laser writing is a powerful tool to reduce many monochromatic aberrations, e.g., by using aspheric surfaces, which provide additional variables in the optical design. Further aberration correction can be achieved using additional optical surfaces, hence, creating multi-lens objectives [4].

However, these compensation methods cannot correct for chromatic aberrations, namely, longitudinal chromatic aberration (LCA) and transverse chromatic aberration (TCA). These chromatic aberrations have been observed in the imaging of 3D written micro-lenses and limit their optical performance [4].

To correct them, two approaches are possible, namely, the combination of refractive and diffractive surfaces or the combination of materials with different dispersion characteristics [19]. In the following, we analyze the chromatic aberrations of 3D printed micro-optics and correct them by combining the two commonly used photoresists, IP-S and IP-Dip, to create an achromatic focusing axicon as well as a Fraunhofer doublet. The latter was introduced by Joseph von Fraunhofer in 1817 for the correction of chromatic lens aberrations [20]. The Fraunhofer condition states that achromaticity for two wavelengths is achieved when the Fraunhofer condition is fulfilled: $f_1/f_2 = -\nu_2/\nu_1$, with f_i as the focal lengths of the lenses and ν_i as the Abbe numbers that characterize the refractive index dispersion of the two lens materials.

For simulation and design of the optical elements, detailed knowledge of the dispersion of the two photoresists is crucial. To measure the refractive indices and dispersion, we use an automated Pulfrich refractometer setup [21]. In Table 1, we list the measurement results for the two-photon exposed photoresists.

The measured dispersion curve is depicted in Fig. 1(a), and the resulting Abbe numbers for different photoresists are plotted in Fig. 1(b). The refractive indices at the F -, d -, and C -line (n_F at 486.13 nm, n_d at 587.56 nm, and n_C at 656.27 nm) are calculated using a Sellmeier fit to the measured data points. Using the definition of the Abbe number $\nu = \frac{n_d - 1}{n_F - n_C}$, the Abbe number of IP-S is calculated to 46.2, while the Abbe number of IP-Dip has a lower value of 34.4, indicating stronger dispersion. The refractive index of IP-Dip is also about 0.04 higher than the refractive index of IP-S. The respective Schott catalog numbers of IP-S and IP-Dip are therefore 511462 and 549344.

The beam paths for the singlet and achromatic focusing axicon illuminated with a collimated white-light source are shown in Fig. 2(a). Focusing is achieved by the curved back surface of the axicon. The image produced by the singlet axicon leads to color split rings with different diameters due to the dispersion of the photoresist (TCA). In contrast, the achromatic focusing axicon consists of two photoresists to form an achromatic prism with a focusing surface. To achieve the achromatic focusing axicon, the prism structure is simply rotated around the z axis. The achromatic axicon can compensate for the dispersive effect,

Table 1. Measured Refractive Indices of Photoresists IP-S and IP-Dip between 500 nm and 900 nm

n	$n_{500\text{ nm}}$	$n_{600\text{ nm}}$	$n_{700\text{ nm}}$	$n_{800\text{ nm}}$	$n_{900\text{ nm}}$
IP-S	1.5178	1.5110	1.5065	1.5037	1.5025
IP-Dip	1.5580	1.5478	1.5420	1.5385	1.5360

thus reducing color splitting. The different color rings overlay in the focal plane, resulting in a white ring. The two axicons are fabricated directly on a glass substrate by three-dimensional dip-in lithography using a Photonic Professional GT (NanoScribe GmbH) direct laser writing system. We use a 25 \times objective and create the achromatic axicon with a two-step process writing the first part, then developing and writing the second part on top. The alignment has been realized writing markers on the substrate. On the left side of Fig. 2(b), a microscope image of the singlet axicon consisting of IP-S is depicted. The larger achromatic axicon is shown on the right. The interface between IP-Dip and IP-S can clearly be seen in the side view.

To verify the optical properties, the optical performances of the two axicons are measured. The measurement setup consists of a white-light laser source, a pinhole after which the samples are placed, and a microscope to image the resulting intensity distributions onto a CMOS chip. Figure 2(c) shows the actual measurement of optical performance. The dispersive effect and wavelength-dependent splitting can clearly be observed in the rainbow colors created by the singlet axicon, whereas the achromatic axicon produces a white ring.

In the next step, we create a Fraunhofer doublet to compensate for the longitudinal chromatic aberration (LCA), which occurs using a simple singlet lens. Due to dispersion,

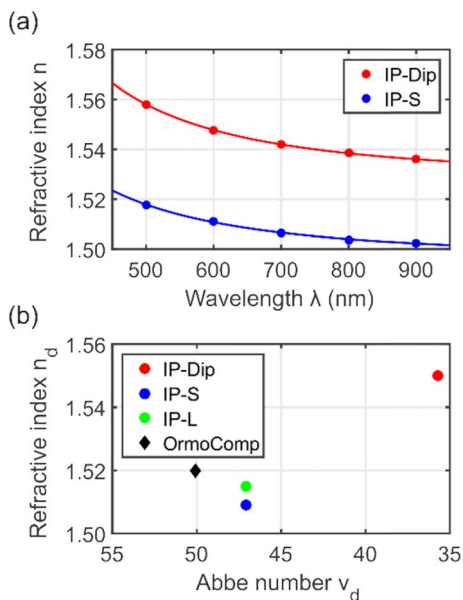


Fig. 1. (a) Refractive index measurements and dispersion of photoresists IP-S and IP-Dip. The Sellmeier equation is fitted to the data points. (b) Abbe diagram containing IP-S, IP-Dip, IP-L, and OrmoComp. The two photoresists IP-S and IP-Dip have different refractive indices and dispersions. Due to the different Abbe numbers, they can be combined to realize achromatic lenses.

the refractive index of the photoresist varies for the different wavelengths. This leads to a change in the focal length depending on the wavelength, which is characterized by the LCA. Figure 3(a) shows the beam path of a singlet lens with prominent LCA. The correction of the beam path using a Fraunhofer doublet is shown in Fig. 3(b). The lens designs are optimized

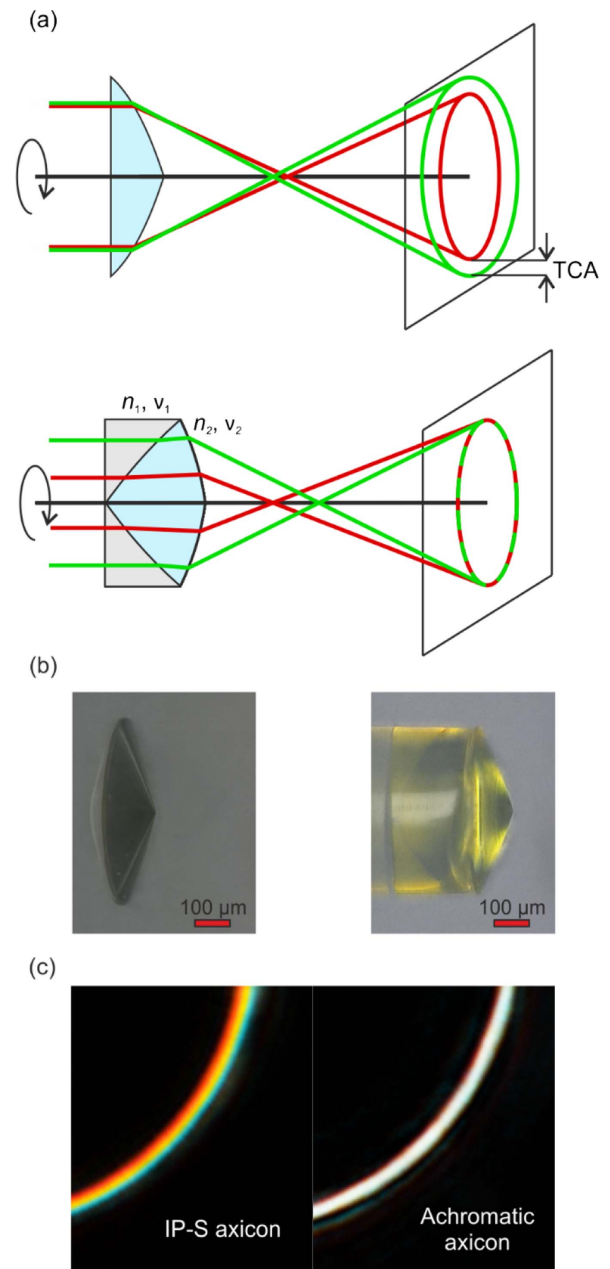


Fig. 2. (a) Design and beam path of the singlet axicon and achromatic axicon (IP-S in blue, IP-Dip in gray). The TCA can clearly be seen in the singlet; in contrast, the achromatic axicon can correct the dispersive effect. (b) Microscope pictures of the singlet axicon (left) and achromatic axicon (right) with a diameter of 500 μm . (c) Measurement results for focal plane intensity distribution of the singlet and achromatic axicon. The dispersive effect and wavelength-dependent splitting can clearly be observed in the rainbow colors created by the singlet axicon, whereas the achromatic axicon produces a white ring.

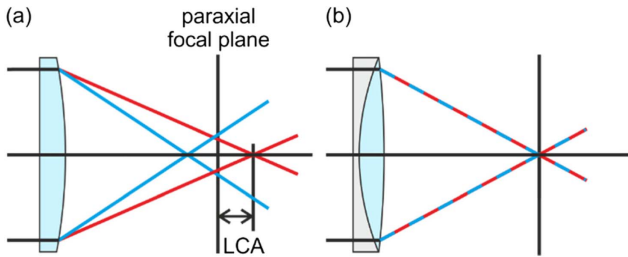


Fig. 3. Ray sketch for (a) singlet lens consisting of IP-S and (b) Fraunhofer doublet combining IP-S and IP-Dip (IP-S in blue, IP-Dip in gray). Due to dispersion, the singlet lens exhibits different focal lengths for different wavelengths (LCA). The Fraunhofer doublet corrects this shift for 500 nm and 700 nm, resulting in the same focal length for both wavelengths.

using the ray-tracing software Zemax with a design focal length of 3 mm and corrected for 500 nm and 700 nm wavelengths.

A microscope image of the 3D-printed Fraunhofer doublet is shown in Fig. 4(a). To measure the LCA, we use the same measurement setup as before. However, this time we use the white-light laser as a variable monochromatic light source at 500 nm, 600 nm, and 700 nm.

We measure the focal length by recording the resulting spot image while changing distance z between lens and microscope for each wavelength, respectively. Resulting spot diagrams using a wavelength of 500 nm are shown in Figs. 4(b)–4(d) at the paraxial focal plane, 100 μm before and behind.

To obtain the intensity distribution along the optical axis, we perform the measurement for each wavelength $\pm 200 \mu\text{m}$ around the designed paraxial focal length and calculate the maximum intensity for each data point. The results are shown in Fig. 5(a) for the singlet and in Fig. 5(b) for the Fraunhofer doublet. The LCA of the singlet can be clearly

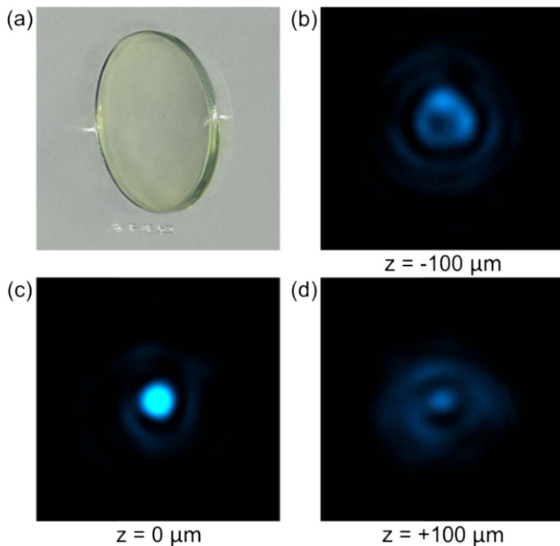


Fig. 4. (a) White-light microscope (Keyence) image of the printed Fraunhofer doublet (diameter 500 μm) and resulting spot diagrams for a wavelength of 500 nm ($\Delta\lambda = 2.2 \text{ nm}$) at -100 μm (b), at the paraxial focal plane (c), and at +100 μm (d). The lateral scale of figure (b)–(d) is 35 μm from edge to edge.

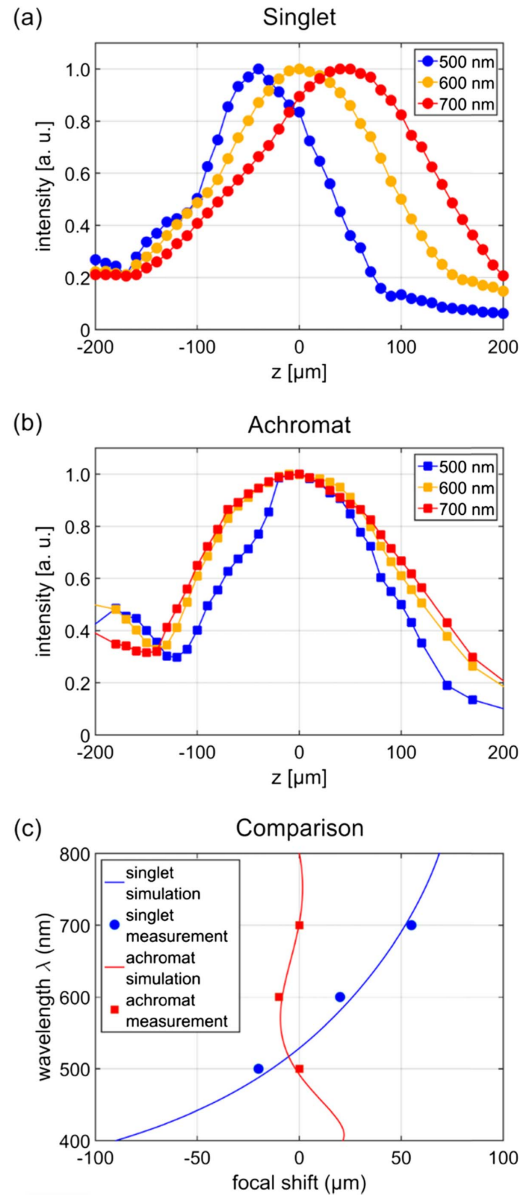


Fig. 5. Through-focus measurement for (a) the singlet lens and (b) the Fraunhofer doublet (both with paraxial focal length $f = 3 \text{ mm}$) at 500 nm, 600 nm, and 700 nm. (c) Simulated and measured LCA of the singlet lens and the Fraunhofer doublet. Simulation and measurement are in good agreement. The reduction of the LCA with the Fraunhofer doublet can be clearly observed, correcting for 500 nm and 700 nm with some secondary aberration visible at 600 nm.

observed by the different maximum intensity positions of the different wavelengths. The focal intensity distributions of the Fraunhofer doublet align much better along the optical axis. To quantify the chromatic aberration, we compare the simulated LCA of the two lens designs with our measurement results in Fig. 5(c). Measurement and simulation show good matching. We observe the typical behavior of the singlet where the focal shift increases with the wavelength. The Fraunhofer doublet exhibits the expected behavior of an achromatic lens, correcting the chromatic aberration at two designed wavelengths (here,

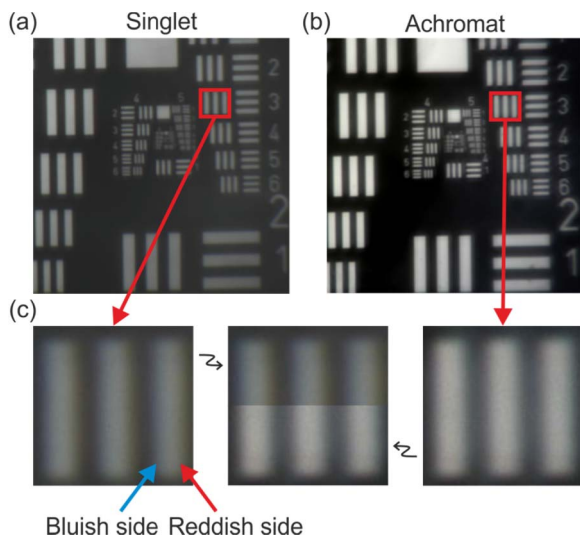


Fig. 6. Imaging of a USAF 1951 test target with the singlet lens (a) and the Fraunhofer doublet (b) showing imaging performance. Illumination is from a halogen light bulb. In the close comparison (c) of the imaging results (third group, element 3) of the singlet and the Fraunhofer doublet, the chromatic error in the image of the singlet lens (left) can clearly be seen, whereas the image of the Fraunhofer doublet (right) compensates for these errors.

500 nm and 700 nm), while the secondary chromatic aberration is still present. It amounts to about 10 μm at 600 nm. Further improvements could be achieved combining three different photoresists to an apochromat or using additional diffractive optical elements.

Figure 6 compares the imaging quality of the singlet lens (a) and the Fraunhofer doublet (b) by imaging a USAF 1951 test target. By magnifying the third element of the third group and analyzing the side-to-side comparison plotted in Fig. 6(c), one can observe the typical transverse chromatic aberrations visible as color seams. The image taken with the Fraunhofer doublet also compensates the transverse chromatic aberration and therefore does not show the color edges. This result proves that combining photoresists with different dispersions is possible, and chromatic aberrations can effectively be reduced, improving the imaging quality significantly.

In summary, we demonstrated the correction of chromatic aberrations by combining two photoresists (IP-S and IP-Dip). As proof of concept, we created an achromatic axicon. We also manufactured a 3D femtosecond-laser-printed Fraunhofer doublet, consisting of IP-S and IP-Dip, which compensates the LCA and improves imaging quality significantly. We demonstrate that multi-component writing is a possible approach for the integration of achromatic functions into 3D-printed micro-optics. The gain in possible optical design freedom is significant and provides a way to enhance imaging quality by reducing chromatic aberrations. Furthermore, this approach

paves the way for the realization of a variety of micro-optical systems using new combinations of photoresists. In the future, secondary chromatic aberration could be even further reduced by combining three or more different photoresists.

Funding. Deutsche Forschungsgemeinschaft (DFG) (GI 269/12-1); Bundesministerium für Bildung und Forschung (BMBF) (13N14097, PRINTOPTICS, PRINTFUNCTION); Baden-Württemberg Stiftung (Spitzenforschung II, OPTERIAL); H2020 European Research Council (ERC) (COMPLEXPLAS).

REFERENCES

1. S. Thiele, T. Gissibl, H. Giessen, and A. M. Herkommer, *Opt. Lett.* **41**, 3029 (2016).
2. S. Thiele, K. Arzenbacher, T. Gissibl, H. Giessen, and A. M. Herkommer, *Sci. Adv.* **3**, e1602655 (2017).
3. P.-I. Dietrich, M. Blaicher, I. Reuter, M. Billah, T. Hoose, A. Hofmann, C. Caer, R. Dangel, B. Offrein, U. Troppenz, M. Moehrl, W. Freude, and C. Koos, *Nat. Photonics* **12**, 241 (2018).
4. T. Gissibl, S. Thiele, A. Herkommer, and H. Giessen, *Nat. Photonics* **10**, 554 (2016).
5. A. Schleunitz, J. J. Klein, R. Houbertz, M. Vogler, and G. Gruetzner, *Proc. SPIE* **9368**, 93680E (2015).
6. A. Schleunitz, J. J. Klein, R. Houbertz, and A. Krupp, *SPIE Newsroom* (2017), <http://www.spie.org/newsroom/6857-novel-hybrid-polymers-for-fabrication-of-advanced-micro-optics?SSO=1>.
7. G. von Freymann, A. Ledermann, M. Thiel, I. Staude, S. Essig, K. Busch, and M. Wegener, *Adv. Funct. Mater.* **20**, 1038 (2010).
8. M. Thiel, A. Radke, B. Fries, D. Eicke, F. Niesler, C. Baretzky, T. Bückmann, M. Wegener, M. Wegener, M. Wegener, M. Thiel, and M. Thiel, in *Conference on Lasers and Electro-Optics (CLEO)* (OSA, 2013), paper ATu2N.4.
9. J.-J. Xu, W.-G. Yao, Z.-N. Tian, L. Wang, K.-M. Guan, Y. Xu, Q.-D. Chen, J.-A. Duan, and H.-B. Sun, *IEEE Photon. Technol. Lett.* **27**, 2465 (2015).
10. T. Gissibl, M. Schmid, and H. Giessen, *Optica* **3**, 448 (2016).
11. Z.-N. Tian, X.-W. Cao, W.-G. Yao, P.-X. Li, Y.-H. Yu, G. Li, Q.-D. Chen, and H.-B. Sun, *IEEE Photon. Technol. Lett.* **28**, 2299 (2016).
12. T. Gissibl, S. Thiele, A. Herkommer, and H. Giessen, *Nat. Commun.* **7**, 11763 (2016).
13. D. Wu, S.-Z. Wu, L.-G. Niu, Q.-D. Chen, R. Wang, J.-F. Song, H.-H. Fang, and H.-B. Sun, *Appl. Phys. Lett.* **97**, 031109 (2010).
14. S. Wong, M. Deubel, F. Pérez-Willard, S. John, G. A. Ozin, M. Wegener, and G. von Freymann, *Adv. Mater.* **18**, 265 (2006).
15. M. Deubel, M. Wegener, S. Linden, G. von Freymann, and S. John, *Opt. Lett.* **31**, 805 (2006).
16. R. Guo, S. Xiao, X. Zhai, J. Li, A. Xia, and W. Huang, *Opt. Express* **14**, 810 (2006).
17. C. Liberale, G. Cojoc, P. Candeloro, G. Das, F. Gentile, F. De Angelis, and E. Di Fabrizio, *IEEE Photon. Technol. Lett.* **22**, 474 (2010).
18. M. Malinauskas, A. Žukauskas, V. Puriys, K. Belazaras, A. Momot, D. Paipulas, R. Gadonas, A. Piskarskas, H. Gilbergs, A. Gaidukevičiūtė, I. Sakellari, M. Farsari, and S. Juodkazis, *J. Opt.* **12**, 124010 (2010).
19. T. Stone and N. George, *Appl. Opt.* **27**, 2960 (1988).
20. J. Fraunhofer, *Ann. Phys.* **56**, 264 (1817).
21. T. Gissibl, S. Wagner, J. Sykora, M. Schmid, and H. Giessen, *Opt. Mater. Express* **7**, 2293 (2017).